A novel general higher-order shear deformation theory for static, vibration and thermal buckling analysis of the functionally graded plates

Trung-Kien Nguyen[a,*], Huu-Tai Thai[b], Thuc P. Vo[c,**]

[a]*Faculty of Civil Engineering, Ho Chi Minh City University of Technology and Education, 1 Vo Van Ngan Street, Thu Duc District, Ho Chi Minh City, Viet Nam*
[b]*Department of Infrastructure Engineering, The University of Melbourne, Parkville VIC 3010, Australia*
[c]*School of Engineering and Mathematical Sciences, La Trobe University, Bundoora, VIC 3086, Australia*

Abstract

This paper proposes a new general framework of higher-order shear deformation theory (HSDT) and solves the structural responses of the functionally graded (FG) plates using novel exponential shape functions for the Ritz method. Based on the fundamental equations of the elasticity theory, the displacement field is expanded in a unified form which can recover to many different shear deformation plate theories such as zeroth-order shear deformation plate theory, third-order shear deformation plate theory, various HSDTs and refined four-unknown HSDTs. The characteristic equations of motion are derived from Lagrange's equations. Ritz-type solutions are developed for bending, free vibration and thermal buckling analysis of the FG plates with various boundary conditions. Three types of temperature variation through the thickness are considered. Numerical results are compared with those from previous studies to verify the accuracy and validity of the present theory. In addition, a parametric study is also performed to investigate the effects of the material parameters, side-to-thickness ratio, temperature rise and boundary conditions on the structural responses of the FG plates.

Keywords: Higher-order shear deformation theory; Functionally graded plates; Static; Vibration; Thermal buckling.

1. Introduction

Plate structures are widely used in engineering field such as mechanical engineering, aerospace, construction, etc. The development of plate theories in order to predict accurately their behaviours has therefore been an interesting topic attracted a number of researches with different approaches. In general, structural responses of the plates can be generally captured by either 2D or 3D theories in

*Corresponding author
**Corresponding author
Email addresses: kiennt@hcmute.edu.vn (Trung-Kien Nguyen), t.vo@latrobe.edu.au (Thuc P. Vo)

which the first approach is more popular owing to its simplicity and low cost computations, whilst the second one is complicated to implement but more accurate. Many shear deformation plate theories have been developed with various displacement fields, only some representative references are herein cited. Based on the single-layer plate theory, in order to account for effects of transverse shear strains, the first-order shear deformation plate theory (FSDT) and higher-order shear deformation plate theory (HSDT) can be employed. In practice, due to simplicity in analysis and programming, the FSDT [1–4] has been mostly used, however a shear correction factor is required. The HSDTs [5–7] with non-linear variations of the membrane displacements or Quasi-3D [8, 9] and Carrera Unified Formulation (CUF) [10–20] with higher-order variations of both membrane and transverse displacements predict more accurate than the FSDT. The novelty of CUF was that it can generate any theories on the basis of the same 'fundamental nucleus' that comes from geometrical relations and Hooke's law [20] and fulfils Koiter's recommendation [21]. It should be noted that the HSDTs neglect the thickness stretching effect, which needs to be considered for functionally graded (FG) plates especially in thermal stresses. This matter was clearly identified and discussed in many CUF papers [12, 13, 16, 18]. However, this is also limitation of this paper, which focuses on a new general framework of HSDTs. The novelty of this framework is that various displacement fields of the plate of existing HSDTs available in the literature could be recovered from this unified theory. In practice, although the higher-order variation of both in-plane and out-of-plane displacements predicts generally more accurate than the HSDTs, it appears to be complicated for implementation and costs due to the increase of variables.

It should be mentioned that the accuracy of HSDTs depends on the selection of shear functions which has been investigated by many researchers. Various types of shear functions have been developed for isotropic, laminated composite and FG plates such as polynomial ([22–26]), trigonometric ([27–33]), exponential ([34]), hyperbolic ([35, 36]), and hybrid ([37, 38]). Among above studies, there are few papers dealing with thermal load. Zenkour and Radwan [9] studied effects of hygro-thermo-mechanical buckling of the FG plates using a Quasi-3D plate theory with a polynomial shear function. Mantari et al. [19] used various plate theories in a unified formulation based on the CUF for analysis of composite plates under thermal load. A brief literature review on the plate theories showed that although a number of researches have been performed, the finding of general models for many different shear deformation plate theories is still essential and this complicated problem needs to be studied further. This is the main contribution of this paper, which proposes a new general framework of HSDT based on the fundamental equations of elasticity theory and then solves the problems by using novel exponential shape functions for the Ritz method.

A new general framework of HSDT, which can recover many available existing theories in the

literature, for static, vibration and thermal buckling analysis of the FG plates is introduced in this paper. The Ritz method is used to approximate solution field within which novel exponential shape functions are introduced for structural analysis of the FG plates with different boundary conditions. Various temperature variations including uniform, linear and nonlinear through the thickness are investigated. Numerical examples for the FG plates are carried out to validate the accuracy and efficiency of the proposed theory. The effects of the material parameters, side-to-thickness ratio, temperature rise and boundary conditions on the structural responses of the FG plates are investigated.

2. Theoretical formulation

2.1. Unified displacement field of the HSDT

Consider a rectangular isotropic plate with sides $a \times b$ and thickness h. Its behaviour is assumed to be elastic, linear and under small displacement. It is assumed that the normal stress is equal to zero, the non-zero transverse shear strains of the plate are calculated via transverse shear stresses and shear modulus $G = E/[2(1+\nu)]$ by:

$$\gamma_{xz} = \frac{\sigma_{xz}}{G} \tag{1a}$$

$$\gamma_{yz} = \frac{\sigma_{yz}}{G} \tag{1b}$$

where E and ν are Young's modulus and Poisson's ratio.

The transverse shear strains in Eq. (1) can be also expressed in terms of membrane and transverse displacements (u, v and w) in x-, y- and $z-$directions of the plate as follows:

$$\gamma_{xz} = u_{,z} + w_{,x} \tag{2a}$$

$$\gamma_{yz} = v_{,z} + w_{,y} \tag{2b}$$

where the comma subscript indicates the differentiation of the variable that follows. Substituting Eq. (2) into Eq. (1) leads to:

$$u_{,z} + w_{,x} = \frac{\sigma_{xz}}{G} \tag{3a}$$

$$v_{,z} + w_{,y} = \frac{\sigma_{yz}}{G} \tag{3b}$$

Moreover, the transverse shear stresses can be obtained from the transverse shear forces, Q_x and Q_y, as follows:

$$\sigma_{xz}(x,y,z) = \Psi'(z)Q_x(x,y) \tag{4a}$$

$$\sigma_{yz}(x,y,z) = \Psi'(z)Q_y(x,y) \tag{4b}$$

where $\Psi(z)$ is a non-linear shear function whose the first derivative satisfies the stress-free conditions at the bottom and top surfaces of the plate, i.e $\Psi'(z = \pm\frac{h}{2}) = 0$. As a special case, $\Psi(z) = \frac{3}{2h}\left(z - \frac{4z^3}{3h^2}\right)$ is common used for the homogeneous plates. In practice, the accuracy of the plate theory strictly depends on a choice of this shear function, which has been studied by many previous authors ([22–38]).

Substituting Eq. (4) into Eq. (3) leads to:

$$u_{,z} + w_{,x} = \frac{\Psi'(z)Q_x(x,y)}{G} \tag{5a}$$

$$v_{,z} + w_{,y} = \frac{\Psi'(z)Q_y(x,y)}{G} \tag{5b}$$

For simplicity purpose, it is assumed that the transverse displacement of the plate is constant through the thickness, i.e $w(x,y,z) = w_0(x,y)$. By integrating Eq. (5) in the thickness direction, the displacement field is obtained as follows:

$$u(x,y,z) = u_0(x,y) - zw_{0,x} + \Psi(z)\frac{Q_x(x,y)}{G} \tag{6a}$$

$$v(x,y,z) = v_0(x,y) - zw_{0,y} + \Psi(z)\frac{Q_y(x,y)}{G} \tag{6b}$$

$$w(x,y,z) = w_0(x,y) \tag{6c}$$

where u_0, v_0 are membrane displacements of the plate. Eq. (6) is a unified framework of the HSDT from which different displacement fields can be found and developed further. As the first case, Eq. (6) is a general zeroth-order shear deformation plate theory. This theory developed by Shimpi [39] for the homogeneous plates and Ray [40] for laminated composite plates can be recovered with $\Psi(z) = \frac{3}{2h}\left(z - \frac{4z^3}{3h^2}\right)$.

Moreover, as a second case, if the transverse shear forces are expressed under the form:

$$Q_x(x,y) = G\varphi_x(x,y) \tag{7a}$$

$$Q_y(x,y) = G\varphi_y(x,y) \tag{7b}$$

where φ_x, φ_y represent as rotations about the y- and x- directions, Eq. (6) becomes:

$$\begin{aligned} u(x,y,z) &= u_0(x,y) - zw_{0,x} + \Psi(z)\varphi_x(x,y) && \text{(8a)} \\ v(x,y,z) &= v_0(x,y) - zw_{0,y} + \Psi(z)\varphi_y(x,y) && \text{(8b)} \\ w(x,y,z) &= w_0(x,y) && \text{(8c)} \end{aligned}$$

It is observed that the displacement field in Eq. (8) is known as a general HSDT which is mostly used in the open literature owing to its simplicity. As a third case, if the transverse shear forces are expressed with the rotation and the derivative of transverse displacement as follows ([23]):

$$\begin{aligned} Q_x(x,y) &= \frac{5Gh}{6}\left(\theta_x + w_{0,x}\right) && \text{(9a)} \\ Q_y(x,y) &= \frac{5Gh}{6}\left(\theta_y + w_{0,y}\right) && \text{(9b)} \end{aligned}$$

Substituting Eq. (9) into Eq. (5) leads to a new general HSDT as:

$$\begin{aligned} u(x,y,z) &= u_0(x,y) + \left(\frac{5h\Psi}{6} - z\right) w_{0,x} + \frac{5h\Psi}{6}\theta_x(x,y) && \text{(10a)} \\ v(x,y,z) &= v_0(x,y) + \left(\frac{5h\Psi}{6} - z\right) w_{0,y} + \frac{5h\Psi}{6}\theta_y(x,y) && \text{(10b)} \\ w(x,y,z) &= w_0(x,y) && \text{(10c)} \end{aligned}$$

It should be noted that the HSDTs derived from Reissner [23], Shi [41] and Reddy [42] can be found in Eq. (10) with $\Psi(z) = \frac{3}{2h}\left(z - \frac{4z^3}{3h^2}\right)$ and $\Psi(z) = \frac{6}{5h}\left(z - \frac{4z^3}{3h^2}\right)$, respectively.

In addition, as a fourth case, if the transverse displacement is decomposed into bending part and shear one as follows: $w_0(x,y) = w_b(x,y) + w_s(x,y)$ and $\theta_x = w_{s,x}, \theta_y = w_{s,y}$, a novel general refined four-unknown HSDT is formulated as follows:

$$\begin{aligned} u(x,y,z) &= u_0(x,y) + \left(\frac{5h\Psi}{6} - z\right) w_{b,x} + \left(\frac{5h\Psi}{3} - z\right) w_{s,x} && \text{(11a)} \\ v(x,y,z) &= v_0(x,y) + \left(\frac{5h\Psi}{6} - z\right) w_{b,y} + \left(\frac{5h\Psi}{3} - z\right) w_{s,y} && \text{(11b)} \\ w(x,y,z) &= w_b(x,y) + w_s(x,y) && \text{(11c)} \end{aligned}$$

2.2. Strains and stresses

In order to derive the characteristic equations of motion of the plate, the displacement field given in Eq. (10) is used in the following theoretical formulations. The non-zero membrane and shear strains associated to the displacements in Eq. (10) are expressed by:

$$\left\{\begin{array}{c}\epsilon_x\\ \epsilon_y\\ \gamma_{xy}\end{array}\right\} = \left\{\begin{array}{c}\epsilon_x^{(0)}\\ \epsilon_y^{(0)}\\ \gamma_{xy}^{(0)}\end{array}\right\} + \Phi_1(z)\left\{\begin{array}{c}\epsilon_x^{(1)}\\ \epsilon_y^{(1)}\\ \gamma_{xy}^{(1)}\end{array}\right\} + \Phi_2(z)\left\{\begin{array}{c}\epsilon_x^{(2)}\\ \epsilon_y^{(2)}\\ \gamma_{xy}^{(2)}\end{array}\right\} \tag{12a}$$

$$\left\{\begin{array}{c}\gamma_{xz}\\ \gamma_{yz}\end{array}\right\} = \Phi_3(z)\left\{\begin{array}{c}\gamma_{xz}^{(0)}\\ \gamma_{yz}^{(0)}\end{array}\right\} \tag{12b}$$

where $\Phi_1(z) = 5h\Psi/6 - z$, $\Phi_2(z) = 5h\Psi/6$, $\Phi_3(z) = 5h\Psi'(z)/6$; and the strains components are calculated by:

$$\left\{\begin{array}{c}\epsilon_x^{(0)}\\ \epsilon_y^{(0)}\\ \gamma_{xy}^{(0)}\end{array}\right\} = \left\{\begin{array}{c}u_{0,x}\\ v_{0,y}\\ u_{0,y}+v_{0,x}\end{array}\right\}, \left\{\begin{array}{c}\epsilon_x^{(1)}\\ \epsilon_y^{(1)}\\ \gamma_{xy}^{(1)}\end{array}\right\} = \left\{\begin{array}{c}w_{0,xx}\\ w_{0,yy}\\ 2w_{0,xy}\end{array}\right\}, \left\{\begin{array}{c}\epsilon_x^{(2)}\\ \epsilon_y^{(2)}\\ \gamma_{xy}^{(2)}\end{array}\right\} = \left\{\begin{array}{c}\theta_{x,x}\\ \theta_{y,y}\\ \theta_{x,y}+\theta_{y,x}\end{array}\right\} \tag{13a}$$

$$\left\{\begin{array}{c}\gamma_{xz}^{(0)}\\ \gamma_{yz}^{(0)}\end{array}\right\} = \left\{\begin{array}{c}\theta_x + w_{0,x}\\ \theta_y + w_{0,y}\end{array}\right\} \tag{13b}$$

The non-zero stresses of the plate associated to the strains in Eq. (12) are given by:

$$\left\{\begin{array}{c}\sigma_x\\ \sigma_y\\ \gamma_{xy}\end{array}\right\} = \left(\begin{array}{ccc}Q_{11} & Q_{12} & 0\\ Q_{12} & Q_{22} & 0\\ 0 & 0 & Q_{66}\end{array}\right)\left\{\begin{array}{c}\epsilon_x\\ \epsilon_y\\ \gamma_{xy}\end{array}\right\} = \mathbf{Q}\boldsymbol{\epsilon} \tag{14a}$$

$$\left\{\begin{array}{c}\sigma_{xz}\\ \sigma_{yz}\end{array}\right\} = \left(\begin{array}{cc}Q_{55} & 0\\ 0 & Q_{44}\end{array}\right)\left\{\begin{array}{c}\gamma_{xz}\\ \gamma_{yz}\end{array}\right\} = \mathbf{Q}^s\boldsymbol{\gamma} \tag{14b}$$

where Q_{ij} and Q_{ij}^s are the reduced stiffness components of the plate which are given by:

$$Q_{11} = Q_{22} = \frac{E}{1-\nu^2}, Q_{12} = \nu Q_{11}, Q_{44} = Q_{55} = Q_{66} = \frac{E}{2(1+\nu)} \tag{15}$$

2.3. Energy formulation

The strain energy $\mathcal{U}$ of the plate is given by:

$$\begin{aligned}
\mathcal{U} &= \frac{1}{2}\int_V (\sigma_x\epsilon_x + \sigma_y\epsilon_y + \sigma_{xy}\gamma_{xy} + \sigma_{xz}\gamma_{xz} + \sigma_{yz}\gamma_{yz})dV \qquad (16)\\
&= \frac{1}{2}\int_A \Big[A_{11}u_{0,x}^2 + A_{22}v_{0,y}^2 + D_{11}w_{0,xx}^2 + D_{22}w_{0,yy}^2 + H_{11}^s\theta_{x,x}^2 + H_{22}^s\theta_{y,y}^2\\
&+ 2B_{11}u_{0,x}w_{0,xx} + 2B_{22}v_{0,y}w_{0,yy} + 2B_{11}^s u_{0,x}\theta_{x,x} + 2B_{22}^s v_{0,y}\theta_{y,y} + 2D_{11}^s w_{0,xx}\theta_{x,x}\\
&+ 2D_{22}^s w_{0,yy}\theta_{y,y} + u_{0,x}(A_{12}v_{0,y} + B_{12}w_{0,yy} + B_{12}^s\theta_{y,y}) + w_{0,xx}(B_{12}v_{0,y} + D_{12}w_{0,yy} + D_{12}^s\theta_{y,y})\\
&+ \theta_{x,x}(B_{12}^s v_{0,y} + D_{12}^s w_{0,yy} + H_{12}^s\theta_{y,y}) + A_{66}(u_{0,y} + v_{0,x})^2 + 4D_{66}w_{0,xy}^2\\
&+ H_{66}^s(\theta_{x,y} + \theta_{y,x})^2 + 4B_{66}w_{0,xy}(u_{0,y} + v_{0,x}) + 2B_{66}^s(u_{0,y} + v_{0,x})(\theta_{x,y} + \theta_{y,x})\\
&+ 4D_{66}^s w_{0,xy}(\theta_{x,y} + \theta_{y,x}) + A_{44}^s(\theta_y + w_{0,y})^2 + A_{55}^s(\theta_x + w_{0,x})^2\Big]dA \qquad (17)
\end{aligned}$$

where A_{ij}, B_{ij}, D_{ij}, B_{ij}^s, D_{ij}^s, H_{ij}^s and A_{ij}^s are the stiffness components of the plates given by:

$$\begin{aligned}
\left(A_{ij}, B_{ij}, D_{ij}, B_{ij}^s, D_{ij}^s, H_{ij}^s\right) &= \int_{-h/2}^{h/2}\left(1, \Phi_1, \Phi_1^2, \Phi_2, \Phi_1\Phi_2, \Phi_2^2\right)Q_{ij}dz \qquad (18a)\\
A_{ij}^s &= \int_{-h/2}^{h/2}\Phi_3^2 Q_{ij}^s dz \qquad (18b)
\end{aligned}$$

The work done $\mathcal{V}$ by a transverse q and in-plane load is determined by ([42]):

$$\mathcal{V} = -\int_A qw_0 dA + \frac{1}{2}\int_A (N_x^0 w_{0,x}^2 + 2N_{xy}^0 w_{0,xy}^2 + N_y^0 w_{0,y}^2)dA \qquad (19)$$

where N_x^0, N_y^0, N_{xy}^0 are in-plane edge loads. For thermal buckling, the pre-buckling in-plane thermal loads are determined by:

$$N_{xy}^0 = 0, N_x^0 = N_y^0 = N^0 = -\int_{h/2}^{h/2}(Q_{11} + Q_{12})\alpha\Delta T dz \qquad (20)$$

where α is the coefficient of thermal expansion; $\Delta T = T(z) - T_0$ is the difference of current temperature with reference one T^0.

The kinetic energy $\mathcal{K}$ of the plate is calculated by:

$$\begin{aligned}
\mathcal{K} &= \frac{1}{2}\int_V \rho(z)\Big(\dot{u}^2 + \dot{v}^2 + \dot{w}^2\Big)dV\\
&= \frac{1}{2}\int_A \Big[I_0(\dot{u}_0^2 + \dot{v}_0^2) + 2I_1(\dot{u}_0 w_{0,x} + \dot{v}_0 w_{0,y}) + 2J_1(\dot{u}_0\dot{\theta}_x + \dot{v}_0\dot{\theta}_y)\\
&+ I_2(\dot{w}_{0,x}^2 + \dot{w}_{0,y}^2) + 2J_2(\dot{w}_{0,x}\dot{\theta}_x + \dot{w}_{0,y}\dot{\theta}_y) + K_2(\dot{\theta}_x^2 + \dot{\theta}_y^2) + I_0\dot{w}_0^2\Big]dA \qquad (21)
\end{aligned}$$

where the dot-superscript indicates the time derivative; ρ is the mass density; and the moments of inertia terms are defined as:

$$\left(I_0, I_1, I_2, J_1, J_2, K_2\right) = \int_{-h/2}^{h/2}\left(1, \Phi_1, \Phi_1^2, \Phi_2, \Phi_1\Phi_2, \Phi_2^2\right)\rho dz \qquad (22)$$

The total energy Π of the plate is calculated by:

$$\begin{aligned}
\Pi &= \frac{1}{2}\int_A \Big[A_{11}u_{0,x}^2 + A_{22}v_{0,y}^2 + D_{11}w_{0,xx}^2 + D_{22}w_{0,yy}^2 + H_{11}^s\theta_{x,x}^2 + H_{22}^s\theta_{y,y}^2 \\
&+ 2B_{11}u_{0,x}w_{0,xx} + 2B_{22}v_{0,y}w_{0,yy} + 2B_{11}^s u_{0,x}\theta_{x,x} + 2B_{22}^s v_{0,y}\theta_{y,y} + 2D_{11}^s w_{0,xx}\theta_{x,x} \\
&+ 2D_{22}^s w_{0,yy}\theta_{y,y} + u_{0,x}(A_{12}v_{0,y} + B_{12}w_{0,yy} + B_{12}^s\theta_{y,y}) + w_{0,xx}(B_{12}v_{0,y} + D_{12}w_{0,yy} + D_{12}^s\theta_{y,y}) \\
&+ \theta_{x,x}(B_{12}^s v_{0,y} + D_{12}^s w_{0,yy} + H_{12}^s\theta_{y,y}) + A_{66}(u_{0,y} + v_{0,x})^2 + 4D_{66}w_{0,xy}^2 + H_{66}^s(\theta_{x,y} + \theta_{y,x})^2 \\
&+ 4B_{66}w_{0,xy}(u_{0,y} + v_{0,x}) + 2B_{66}^s(u_{0,y} + v_{0,x})(\theta_{x,y} + \theta_{y,x}) + 4D_{66}^s w_{0,xy}(\theta_{x,y} + \theta_{y,x}) \\
&+ A_{44}^s(\theta_y + w_{0,y})^2 + A_{55}^s(\theta_x + w_{0,x})^2\Big]dA - \int_A \Big[qw_0 + N^0(w_{0,x}^2 + w_{0,y}^2)\Big]dA \\
&- \frac{1}{2}\int_A \Big[I_0(\dot{u}_0^2 + \dot{v}_0^2) + 2I_1(\dot{u}_0 w_{0,x} + \dot{v}_0 w_{0,y}) + 2J_1(\dot{u}_0\dot{\theta}_x + \dot{v}_0\dot{\theta}_y) \\
&+ I_2(\dot{w}_{0,x}^2 + \dot{w}_{0,y}^2) + 2J_2(\dot{w}_{0,x}\dot{\theta}_x + \dot{w}_{0,y}\dot{\theta}_y) + K_2(\dot{\theta}_x^2 + \dot{\theta}_y^2) + I_0\dot{w}_0^2\Big]dA
\end{aligned} \tag{23}$$

2.4. Ritz-type solution

By using novel exponential shape functions, the displacement variables can be approximated as follows:

$$u_0(x,y,t) = \sum_{i=1}^{n_x}\sum_{j=1}^{n_y} u_{ij}(t)R_{i,x}(x)P_j(y) \tag{24a}$$

$$v_0(x,y,t) = \sum_{i=1}^{n_x}\sum_{j=1}^{n_y} v_{ij}(t)R_i(x)P_{j,y}(y) \tag{24b}$$

$$w_0(x,y,t) = \sum_{i=1}^{n_x}\sum_{j=1}^{n_y} w_{ij}(t)R_i(x)P_j(y) \tag{24c}$$

$$\theta_x(x,y,t) = \sum_{i=1}^{n_x}\sum_{j=1}^{n_y} x_{ij}(t)R_{i,x}(x)P_j(y) \tag{24d}$$

$$\theta_y(x,y,t) = \sum_{i=1}^{n_x}\sum_{j=1}^{n_y} y_{ij}(t)R_i(x)P_{j,y}(y) \tag{24e}$$

where $d_{ij} = (u_{ij}, v_{ij}, w_{ij}, x_{ij}, y_{ij})$ are five unknowns variables; $R_i(x)$ and $P_j(y)$ are the shape functions in x- and $y-$direction associated to the displacements d_{ij}, which are selected in such that the solution variables have the same order. As a result, five unknowns of the plate only depend on two shape functions. It should be noted that the accuracy, convergence rates and numerical instabilities of the Ritz solution depends on the selection of the shape functions, which was discussed in details in [43–48]. In this paper, novel shape functions are proposed in Table 1 in which they are expressed under a hybrid form of exponential functions and admissible polynomial ones that satisfy the boundary conditions (BCs):

- Simply-supported (S): $v_0 = w_0 = \theta_y = 0$ at $x = 0, a$ and $u_0 = w_0 = \theta_x = 0$ at $y = 0, b$
- Clamped (C), $u_0 = v_0 = w_0 = \theta_x = \theta_y = 0$ at $x = 0, a$ and $y = 0, b$.

The combination of simply-supported, clamped and free boundary on the edges of the plate leads to the various BCs as follows: SSSS, CCCC, CSCS, CCSS, CCFF and CCSF, which will be considered in the numerical examples.

By using Lagrange's equation and substituting Eq. (24) into Eq. (23) leads to:

$$\frac{\partial \Pi}{\partial d} - \frac{d}{dt}\frac{\partial \Pi}{\partial \dot{d}} = 0 \tag{25}$$

$$\begin{bmatrix} \mathbf{K}^{11} & \mathbf{K}^{12} & \mathbf{K}^{13} & \mathbf{K}^{14} & \mathbf{K}^{15} \\ {}^{T}\mathbf{K}^{12} & \mathbf{K}^{22} & \mathbf{K}^{23} & \mathbf{K}^{24} & \mathbf{K}^{25} \\ {}^{T}\mathbf{K}^{13} & {}^{T}\mathbf{K}^{23} & \mathbf{K}^{33} & \mathbf{K}^{34} & \mathbf{K}^{35} \\ {}^{T}\mathbf{K}^{14} & {}^{T}\mathbf{K}^{24} & {}^{T}\mathbf{K}^{34} & \mathbf{K}^{44} & \mathbf{K}^{45} \\ {}^{T}\mathbf{K}^{15} & {}^{T}\mathbf{K}^{25} & {}^{T}\mathbf{K}^{35} & {}^{T}\mathbf{K}^{45} & \mathbf{K}^{55} \end{bmatrix} \begin{Bmatrix} \mathbf{u} \\ \mathbf{v} \\ \mathbf{w} \\ \mathbf{x} \\ \mathbf{y} \end{Bmatrix}$$

$$+ \begin{bmatrix} \mathbf{M}^{11} & \mathbf{0} & \mathbf{M}^{13} & \mathbf{M}^{14} & \mathbf{0} \\ \mathbf{0} & \mathbf{M}^{22} & \mathbf{M}^{23} & \mathbf{0} & \mathbf{M}^{25} \\ {}^{T}\mathbf{M}^{13} & {}^{T}\mathbf{M}^{23} & \mathbf{M}^{33} & \mathbf{M}^{34} & \mathbf{M}^{35} \\ {}^{T}\mathbf{M}^{14} & \mathbf{0} & {}^{T}\mathbf{M}^{34} & \mathbf{M}^{44} & \mathbf{0} \\ \mathbf{0} & {}^{T}\mathbf{M}^{25} & {}^{T}\mathbf{M}^{35} & \mathbf{0} & \mathbf{M}^{55} \end{bmatrix} \begin{Bmatrix} \ddot{\mathbf{u}} \\ \ddot{\mathbf{v}} \\ \ddot{\mathbf{w}} \\ \ddot{\mathbf{x}} \\ \ddot{\mathbf{y}} \end{Bmatrix} = \begin{Bmatrix} \mathbf{0} \\ \mathbf{0} \\ \mathbf{f} \\ \mathbf{0} \\ \mathbf{0} \end{Bmatrix} \tag{26}$$

or under the compact form as follows:

$$\mathbf{K}\mathbf{d} + \mathbf{M}\ddot{\mathbf{d}} = \mathbf{F} \tag{27}$$

where $\mathbf{K}$, $\mathbf{M}$ and $\mathbf{F}$ are obtained as follows:

$$
\begin{aligned}
K_{ijkl}^{11} &= A_{11}T_{ik}^{22}S_{jl}^{00} + A_{66}T_{ik}^{11}S_{jl}^{11}, K_{ijkl}^{12} = A_{12}T_{ik}^{20}S_{jl}^{02} + A_{66}T_{ik}^{11}S_{jl}^{11} \\
K_{ijkl}^{13} &= B_{11}T_{ik}^{22}S_{jl}^{00} + B_{12}T_{ik}^{20}S_{jl}^{02} + 2B_{66}T_{ik}^{11}S_{jl}^{11} \\
K_{ijkl}^{14} &= B_{11}^{s}T_{ik}^{22}S_{jl}^{00} + B_{66}^{s}T_{ik}^{11}S_{jl}^{11}, K_{ijkl}^{15} = B_{12}^{s}T_{ik}^{20}S_{jl}^{02} + B_{66}^{s}T_{ik}^{11}S_{jl}^{11} \\
K_{ijkl}^{22} &= A_{22}T_{ik}^{00}S_{jl}^{22} + A_{66}T_{ik}^{11}S_{jl}^{11}, K_{ijkl}^{24} = B_{12}^{s}T_{ik}^{02}S_{jl}^{20} + B_{66}^{s}T_{ik}^{11}S_{jl}^{11} \\
K_{ijkl}^{23} &= B_{22}T_{ik}^{00}S_{jl}^{22} + B_{12}T_{ik}^{02}S_{jl}^{20} + 2B_{66}T_{ik}^{11}S_{jl}^{11} \\
K_{ijkl}^{25} &= B_{22}^{s}T_{ik}^{00}S_{jl}^{22} + B_{66}^{s}T_{ik}^{11}S_{jl}^{11} \\
K_{ijkl}^{33} &= D_{11}T_{ik}^{22}S_{jl}^{00} + D_{22}T_{ik}^{00}S_{jl}^{22} + 2D_{12}T_{ik}^{20}S_{jl}^{02} + 4D_{66}T_{ik}^{11}S_{jl}^{11} + A_{44}^{s}T_{ik}^{00}S_{jl}^{11} + A_{55}^{s}T_{ik}^{11}S_{jl}^{00} \\
&+ N^{0}(T_{ik}^{11}S_{jl}^{00} + T_{ik}^{00}S_{jl}^{11}) \\
K_{ijkl}^{34} &= D_{11}^{s}T_{ik}^{22}S_{jl}^{00} + D_{12}^{s}T_{ik}^{02}S_{jl}^{20} + 2D_{66}^{s}T_{ik}^{11}S_{jl}^{11} + A_{55}^{s}T_{ik}^{11}S_{jl}^{00} \\
K_{ijkl}^{35} &= D_{22}^{s}T_{ik}^{00}S_{jl}^{22} + D_{12}^{s}T_{ik}^{20}S_{jl}^{02} + 2D_{66}^{s}T_{ik}^{11}S_{jl}^{11} + A_{44}^{s}T_{ik}^{00}S_{jl}^{11} \\
K_{ijkl}^{44} &= H_{11}^{s}T_{ik}^{22}S_{jl}^{00} + H_{66}^{s}T_{ik}^{11}S_{jl}^{11} + A_{55}^{s}T_{ik}^{11}S_{jl}^{00}, K_{ijkl}^{45} = H_{12}^{s}T_{ik}^{20}S_{jl}^{02} + H_{66}^{s}T_{ik}^{11}S_{jl}^{11} \\
K_{ijkl}^{55} &= H_{22}^{s}T_{ik}^{00}S_{jl}^{22} + H_{66}^{s}T_{ik}^{11}S_{jl}^{11} + A_{44}^{s}T_{ik}^{00}S_{jl}^{11} \\
M_{ijkl}^{11} &= I_{0}T_{ik}^{11}S_{jl}^{00}, M_{ijkl}^{13} = I_{1}T_{ik}^{11}S_{jl}^{00}, M_{ijkl}^{14} = J_{1}T_{ik}^{11}S_{jl}^{00} \\
M_{ijkl}^{22} &= I_{0}T_{ik}^{00}S_{jl}^{11}, M_{ijkl}^{23} = I_{1}T_{ik}^{00}S_{jl}^{11}, M_{ijkl}^{25} = J_{1}T_{ik}^{00}S_{jl}^{11} \\
M_{ijkl}^{33} &= I_{2}(T_{ik}^{11}S_{jl}^{00} + T_{ik}^{00}S_{jl}^{11}) + I_{0}T_{ik}^{00}S_{jl}^{00}, M_{ijkl}^{34} = J_{2}T_{ik}^{11}S_{jl}^{00}, M_{ijkl}^{35} = J_{2}T_{ik}^{00}S_{jl}^{11} \\
M_{ijkl}^{44} &= K_{2}T_{ik}^{11}S_{jl}^{00}, M_{ijkl}^{55} = K_{2}T_{ik}^{00}S_{jl}^{11}, f_{ij} = f_{ij}^{00}
\end{aligned} \tag{28}
$$

with

$$
T_{ik}^{mn} = \int_0^a \frac{\partial^m R_i}{\partial x^m}\frac{\partial^n R_k}{\partial x^n}dx, S_{jl}^{mn} = \int_0^b \frac{\partial^m P_j}{\partial y^m}\frac{\partial^n P_l}{\partial y^n}dy, f_{ij}^{00} = \int_0^a\int_0^b qR_iP_jdxdy \tag{29}
$$

It is worth to noticing that for static analysis under mechanical loads, the displacement and stress responses of the plate can be obtained from Eq. (27) by setting $\mathbf{M} = \mathbf{0}$. For vibration analysis, by denoting $\mathbf{d}(t) = \mathbf{d}e^{i\omega t}$ where ω is the natural frequency of the plate and $i^2 = -1$ is imaginary unit, the natural frequency can be derived from the following equation $(\mathbf{K} - \omega^2\mathbf{M})\mathbf{d} = \mathbf{0}$. For thermal analysis, the critical buckling temperature can be obtained by solving the characteristic equation $\det(\mathbf{K}) = 0$.

2.5. Material properties and temperature distribution

Consider a FG plate made of Al/ZrO_2 and Al/Al_2O_3 with the material properties in Table 2. For FGMs, Ostoja-Starzewski et al. [49–51] presented a method based on micromechanics to calculate the effective macroscopic properties, which required processing of several length scales: a thin interfacial

microstructure, its mesocontinuous representation, fiber size and macroscale level. They demonstrated the bounding of the effective properties of random multiscale microstructures by means of essential and natural boundary conditions [52] and also measured the fractal dimension of phase interfaces in two-phase FGM [53]. However, in this paper with assumption weak mismatches between the phases and using power-law model that presented by Reddy [42], the effective elastic properties are estimated as follows:

$$P(z) = (P_t - P_b)\left(\frac{z}{h} + \frac{1}{2}\right)^p + P_b \tag{30}$$

where p is material parameter or power-law index; P_t, P_b are the material properties at the top and bottom of plate.

For the temperature field, three different types of temperature variations are considered as below.

- For the uniform temperature rise (UTR): the expression of the current temperature is derived from a reference temperature at the bottom surface T_0 as:

$$T(z) = T_0 + \Delta T \tag{31}$$

- For the linear temperature rise (LTR): the expression of the current temperature is calculated based on the temperatures at the top plate surface T_t and bottom plate surface T_b as follows:

$$T(z) = (T_t - T_b)\left(\frac{z}{h} + \frac{1}{2}\right) + T_b \tag{32}$$

- For the nonlinear temperature rise (NLTR): the expression of the current temperature is derived from the coefficient of thermal conductivity $k(z)$ based on the Fourier equation of steady-state heat conduction as follows:

$$T(z) = T_b + \frac{T_t - T_b}{\int_{-h/2}^{h/2} 1/k(z)dz}\int_{-h/2}^{z}\frac{1}{k(\xi)d\xi} \tag{33}$$

3. Numerical examples

In this section, the FG plates in Fig. 1 with the shear function $\Psi(z) = \cot^{-1}\frac{h}{z} - \frac{16z^3}{15h^3}$ [45] are analysed for the proposed HSDT. Numerical examples are reported to verify the validity of the present solutions and investigate the effects of side-to-thickness ratio a/h, material parameter p and boundary conditions (BCs) as well as the variation of temperature field on the structural responses of the FG

plates. For convenience, the following normalized parameters are used:

$$\bar{u} = \frac{100E_c h^3}{q_0 a^4} u\left(0, \frac{b}{2}, z\right), \bar{w} = \frac{10E_c h^3}{q_0 a^4} w\left(\frac{a}{2}, \frac{b}{2}\right), \hat{w} = \frac{100E_m h^3}{12(1-\nu_m^2) q_0 a^4} w\left(\frac{a}{2}, \frac{b}{2}\right) \quad (34a)$$

$$\bar{\sigma}_x(z) = \frac{h}{q_0 a} \sigma_x\left(\frac{a}{2}, \frac{b}{2}, z\right), \bar{\sigma}_{xy}(z) = \frac{h}{q_0 a} \sigma_{xz}\left(0, 0, z\right), \bar{\sigma}_{xz}(z) = \frac{h}{q_0 a} \sigma_{xz}\left(0, \frac{b}{2}, z\right) \quad (34b)$$

$$\bar{\omega} = \frac{\omega a b}{\pi^2 h} \sqrt{\frac{12(1-\nu_c^2)\rho_c}{E_c}} \quad (34c)$$

$$\bar{T}_{cr} = \Delta T_{cr} \times 10^{-3} \quad (34d)$$

For convergence study, Table 3 shows nondimensional transverse displacement $\hat{w}$ and fundamental frequency $\bar{\omega}$ of the Al/ZrO_2-2 square plates under a uniformly distributed load with $a/h = 5$ and $p = 2$. The results are calculated with six types of BCs (CCCC, SSSS, CCSS, CSCS, CCSF, CCFF) and the same number of series in $x-$ and $y-$direction ($n_x = n_y = n$). It can be seen from Table 3 that the results converge very quickly, and the number of series $n = 10$ is sufficient for convergence of the static and dynamic responses of the FG plates. Therefore, the number of series $n = 10$ is assumed to be a convergence point of the solution field and will be used hereafter for numerical computations.

The first verification study is performed for a simply-suported FG plate subjected to a sinusoidal load with $a/h = 10$. The aim of this example is to validate the accuracy of the derived solutions and the proposed theory in predicting the bending responses of Al/Al_2O_3 plates. Table 4 summarises the nondimensional membrane displacements, transverse displacements, membrane stresses and transverse stresses of the considered plate obtained from the present study and those generated by Zenkour [5] based on a sinusoidal shear deformation theory (SSDT), Thai and Kim [6] based on a hyperbolic shear deformable theory (HSDT) and Carrera et al. [11] based on a CUF model. It can be observed that the present solutions are in good agreement with previous ones.

The next verification study aims at verifying the accuracy of the present solutions for the FG plates with different BCs. A square Al/ZrO_2-1 plate subjected to uniformly distributed load is considered with various $p = 0, 0.5, 1, 2, 5, 10$ and $a/h = 5, 10$. The obtained deflections are compared with those predicted by the FSDT [3] and [2], and Quasi-3D theory [8] for SSSS, CCCC and CCSS plates as shown in Table 5. It can be found that the present results comply with those predicted by the FSDT for all BCs considered. There is a slight difference between the present model and Quasi-3D one [8] due to the normal strain effect which is ignored in the present theory. In addition, new results for other BCs predicted by the present theory are also provided in this example to serve as benchmarks for the development of other plate models in the future. It is observed from Table 5 that the center deflection increases as p increases and the maximum and minimum values of the displacement appear in SSSS and CCCC plates, respectively. Furthermore, Figs. 2 and 3 display variations of nondimensional

transverse shear and membrane stresses in the thickness direction of simply-supported Al/ZrO_2-1 plate under uniformly distributed load with various of p and $a/h = 10$. As expected, the shear stress disappears at the top and bottom surfaces of the plate. The maximum stresses tend to slightly move forward to the upper surface of the plate due to asymmetric properties of the FG plates. Whereas, the axial stress increases with p and minimises when $p < 1$. The effects of both a/h and p on the deflection $\bar{w}$ as illustrated in Fig. 4 indicate that the shear deformation effect is much more dominant for very thick plates with a/h less than 5.0.

The aim of the third example is to verify the validity of the present solutions in predicting free vibration responses of the FG plates. A square Al/ZrO_2-2 plate under various BCs is considered in this example. Table 6 shows the comparison of the nondimensional fundamental frequencies for different values of p, $a/h = 5, 10$ and various BCs. The obtained results are compared to those derived from a 3D plate model of Uymaz and Aydodu [54] and a HSDT of Nguyen [7]. It is clear that the normalized fundamental frequencies derived from the present model are in excellent agreement with those from the HSDT and Quasi-3D theory for the SSSS plate, whereas for other BCs there are some slight deviations between them. Table 6 shows that the nondimensional fundamental frequencies decrease with an increase of p. This can be explained by the fact that the increase of p leads to a decrease of the ceramic volume fraction, and thus that makes the plate become softer.

The fourth example aims to evaluate the accuracy of the present theory in predicting thermal buckling behaviours. Table 7 summarizes the critical buckling temperatures of simply-supported Al/Al_2O_3 square plates with $a/h = 5$ and 10. The results are obtained for three types of temperature rise (UTR, LTR, NLTR) in which it is assumed that the reference temperature is taken at the bottom surface of the plate. The obtained results are compared with those obtained from the FSDT [4], HSDT and Quasi-3D theory from [9]. It is observed that there are excellent agreement of the results between the HSDT models for all values of p and a/h. There is a slight difference between the present model and Quasi-3D one observed in the case of thick plate. This is again due to effects of the transverse and shear normal strains which included in Quasi-3D model, but ignored here. Moreover, the effects of BCs and p on the critical buckling temperatures of the Al/Al_2O_3 plate are also plotted in Fig. 5, in which the results are computed for three representative BCs (SSSS, CCCC, CCSS) for $a/h = 10$ and UTR. The results decrease rapidly from $p \leq 2$ and then the curves become flatter as expected since the variation of ceramic volume fraction led to the decrease of the plate stiffness. Furthermore, the effect of temperature rise (UTR, LTR, NLTR) with respect to p is displayed in Fig. 6 for the simply-supported Al/Al_2O_3 square plate with $a/h = 10$. The highest and lower ones correspond to the NLTR and UTR. The results of LTR and NLTR is similar for the homogeneous plate ($p = 0$).

Additionally, the effects of temperature change on fundamental frequencies are also investigated in Fig. 7 with $a/h = 5$ and $p = 5$. Three frequency-temperature interaction curves are plotted for UTR, LTR and NLTR. It can be seen that the natural frequency diminishes with an increase of the temperature. The maximum and minimum critical buckling temperatures are again found for NLTR and UTR, respectively.

4. Conclusions

Based on the fundamental equations of elasticity theory, a novel general HSDT is proposed in this paper for the FG plates. Different displacement fields of the plate of existing HSDTs available in the literature could be recovered from this unified theory. Characteristic governing equations of the plate are derived. They are then solved for approximate solutions using the Ritz method and Lagrange's equations. Novel exponential shape functions are used to solve the static, free vibration and thermal buckling problems. The verification study indicates that the present model can provide an accurate prediction for strucural responses of the FG plates under different geometric configurations and material parameters. New results are also presented as benchmarks for the future comparison with other plate models.

Acknowledgements

This research is funded by Vietnam National Foundation for Science and Technology Development (NAFOSTED) under Grant No. 107.02-2018.312.

References

[1] T. K. Nguyen, K. Sab, G. Bonnet, First-order shear deformation plate models for functionally graded materials, Composite Structures 83 (2008) 25–36.

[2] H. Nguyen-Xuan, L. V. Tran, T. Nguyen-Thoi, H. Vu-Do, Analysis of functionally graded plates using an edge-based smoothed finite element method, Composite Structures 93 (11) (2011) 3019 – 3039.

[3] Y. Y. Lee, X. Zhao, K. M. Liew, Thermoelastic analysis of functionally graded plates using the element-free kp-ritz method, Smart Materials and Structures 18 (3) (2009) 035007.

[4] H. Yaghoobi, M. Torabi, Exact solution for thermal buckling of functionally graded plates resting on elastic foundations with various boundary conditions, Journal of Thermal Stresses 36 (9) (2013) 869–894.

[5] A. M. Zenkour, Generalized shear deformation theory for bending analysis of functionally graded plates, Applied Mathematical Modelling 30 (1) (2006) 67 – 84.

[6] H. T. Thai, S. E. Kim, A simple higher-order shear deformation theory for bending and free vibration analysis of functionally graded plates, Composite Structures 96 (2013) 165–173.

[7] T.-K. Nguyen, A higher-order hyperbolic shear deformation plate model for analysis of functionally graded materials, International Journal of Mechanics and Materials in Design 11 (2) (2015) 203–219.

[8] D. Gilhooley, R. Batra, J. Xiao, M. McCarthy, J. Gillespie, Analysis of thick functionally graded plates by using higher-order shear and normal deformable plate theory and mlpg method with radial basis functions, Composite Structures 80 (4) (2007) 539 – 552.

[9] A. M. Zenkour, A. F. Radwan, Hygrothermo-mechanical buckling of fgm plates resting on elastic foundations using a quasi-3d model, International Journal for Computational Methods in Engineering Science and Mechanics 20 (2) (2019) 85–98.

[10] E. Carrera, Theories and finite elements for multilayered plates and shells:a unified compact formulation with numerical assessment and benchmarking, Archives of Computational Methods in Engineering 10 (3) (2003) 215–296.

[11] E. Carrera, S. Brischetto, A. Robaldo, Variable kinematic model for the analysis of functionally graded material plates, AIAA Journal 46 (1) (2008) 194 – 203.

[12] S. Brischetto, R. Leetsch, E. Carrera, T. Wallmersperger, B. Kröplin, Thermo-Mechanical Bending of Functionally Graded Plates, Journal of Thermal Stresses 31 (3) (2008) 286–308. doi:10.1080/01495730701876775.

[13] M. Cinefra, E. Carrera, S. Brischetto, S. Belouettar, Thermo-Mechanical Analysis Of Functionally Graded Shells, Journal of Thermal Stresses 33 (10) (2010) 942–963. doi:10.1080/01495739.2010.482379.

[14] E. Carrera, F. Miglioretti, M. Petrolo, Accuracy of refined finite elements for laminated plate analysis, Composite Structures 93 (5) (2011) 1311 – 1327.

[15] E. Carrera, S. Brischetto, M. Cinefra, M. Soave, Effects of thickness stretching in functionally graded plates and shells, Composites Part B: Engineering 42 (2) (2011) 123 – 133.

[16] F. A. Fazzolari, E. Carrera, Thermal stability of fgm sandwich plates under various through-the-thickness temperature distributions, Journal of Thermal Stresses 37 (12) (2014) 1449–1481. doi:10.1080/01495739.2014.937251.

[17] E. Carrera, E. Zappino, Carrera unified formulation for free-vibration analysis of aircraft structures, AIAA Journal 54 (1) (2016) 280–292.

[18] I. A. Ramos, J. L. Mantari, A. Pagani, E. Carrera, Refined theories based on non-polynomial kinematics for the thermoelastic analysis of functionally graded plates, Journal of Thermal Stresses 39 (7) (2016) 835–853. doi:10.1080/01495739.2016.1189771.

[19] J. L. Mantari, I. A. Ramos, A. M. Zenkour, A unified formulation for laminated composite and sandwich plates subject to thermal load using various plate theories, International Journal of Applied Mechanics 08 (08) (2016) 1650087.

[20] E. Carrera, M. Cinefra, M. Petrolo, E. Zappino, Finite element analysis of structures through unified formulation, John Wiley & Sons, 2014.

[21] W. T. Koiter, A consistent first approximation in the general theory of thin elastic shells. In: Proceedings of first symposium on the theory of thin elastic shells, North-Holland, Amsterdam.

[22] S. Ambartsumian, On the theory of bending of anisotropic plates and shallow shells, Journal of Applied Mathematics and Mechanics 24 (2) (1960) 500–514.

[23] E. Reissner, On transverse bending of plates, including the effect of transverse shear deformation, International Journal of Solids and Structures 11 (5) (1975) 569–573.

[24] M. Levinson, An accurate, simple theory of the statics and dynamics of elastic plates, Mechanics Research Communications 7 (6) (1980) 343–350.

[25] J. N. Reddy, A Simple Higher-Order Theory for Laminated Composite Plates, Journal of Applied Mechanics 51 (4) (1984) 745–752.

[26] T. N. Nguyen, C. H. Thai, H. Nguyen-Xuan, On the general framework of high order shear deformation theories for laminated composite plate structures: A novel unified approach, International Journal of Mechanical Sciences 110 (2016) 242–255.

[27] M. Murthy, An improved transverse shear deformation theory for laminated anisotropic plates, National Aeronautics and Space Administration, Washington DC, 1981.

[28] M. STEIN, Nonlinear theory for plates and shells including the effects of transverse shearing, AIAA Journal 24 (9) (1986) 1537–1544.

[29] M. Touratier, An efficient standard plate theory, International Journal of Engineering Science 29 (8) (1991) 901–916.

[30] H. Arya, R. Shimpi, N. Naik, A zigzag model for laminated composite beams, Composite Structures 56 (1) (2002) 21–24.

[31] C. H. Thai, A. Ferreira, S. Bordas, T. Rabczuk, H. Nguyen-Xuan, Isogeometric analysis of laminated composite and sandwich plates using a new inverse trigonometric shear deformation theory, European Journal of Mechanics - A/Solids 43 (2014) 89–108.

[32] J. Mantari, A. Oktem, C. G. Soares, A new trigonometric shear deformation theory for isotropic, laminated composite and sandwich plates, International Journal of Solids and Structures 49 (1) (2012) 43–53.

[33] V.-H. Nguyen, T.-K. Nguyen, H.-T. Thai, T. P. Vo, A new inverse trigonometric shear deformation theory for isotropic and functionally graded sandwich plates, Composites Part B: Engineering 66 (2014) 233–246.

[34] M. Aydogdu, A new shear deformation theory for laminated composite plates, Composite Structures 89 (1) (2009) 94–101.

[35] K. P. Soldatos, A transverse shear deformation theory for homogeneous monoclinic plates, Acta Mechanica 94 (3) (1992) 195–220.

[36] S. S. Akavci, A. H. Tanrikulu, Buckling and free vibration analyses of laminated composite plates by using two new hyperbolic shear-deformation theories, Mechanics of Composite Materials 44 (2) (2008) 145–154.

[37] J. Mantari, A. Oktem, C. G. Soares, A new higher order shear deformation theory for sandwich and composite laminated plates, Composites Part B: Engineering 43 (3) (2012) 1489–1499.

[38] C. H. Thai, S. Kulasegaram, L. V. Tran, H. Nguyen-Xuan, Generalized shear deformation theory for functionally graded isotropic and sandwich plates based on isogeometric approach, Computers & Structures 141 (2014) 94–112.

[39] R. P. Shimpi, Zeroth-order shear deformation theory for plates, AIAA Journal 37 (4) (1999) 524–526.

[40] M. C. Ray, Zeroth-Order Shear Deformation Theory for Laminated Composite Plates , Journal of Applied Mechanics 70 (3) (2003) 374–380.

[41] G. Shi, K. Lam, T. Tay, On efficient finite element modeling of composite beams and plates using higher-order theories and an accurate composite beam element, Composite Structures 41 (2) (1998) 159–165.

[42] J. N. Reddy, Mechanics of Laminated Composites Plates: Theory and Analysis, CRC Press, Boca Raton, 1997.

[43] M. Aydogdu, Vibration analysis of cross-ply laminated beams with general boundary conditions by ritz method, International Journal of Mechanical Sciences 47 (11) (2005) 1740 – 1755.

[44] M. Aydogdu, Buckling analysis of cross-ply laminated beams with general boundary conditions by ritz method, Composites Science and Technology 66 (10) (2006) 1248 – 1255.

[45] T.-K. Nguyen, T. T.-P. Nguyen, T. P. Vo, H.-T. Thai, Vibration and buckling analysis of functionally graded sandwich beams by a new higher-order shear deformation theory, Composites Part B: Engineering 76 (2015) 273 – 285.

[46] T.-K. Nguyen, T. P. Vo, B.-D. Nguyen, J. Lee, An analytical solution for buckling and vibration analysis of functionally graded sandwich beams using a quasi-3d shear deformation theory, Composite Structures 156 (2016) 238 – 252, 70th Anniversary of Professor J. N. Reddy.

[47] J. Mantari, F. Canales, Free vibration and buckling of laminated beams via hybrid ritz solution for various penalized boundary conditions, Composite Structures 152 (2016) 306–315.

[48] P. Moreno-García, J. dos Santos, H. Lopes, A review and study on ritz method admissible functions with emphasis on buckling and free vibration of isotropic and anisotropic beams and plates, Archives of Computational Methods in Engineering 25 (2018) 785–815.

[49] M. Ostoja-Starzewski, I. Jasiuk, W. Wang, K. Alzebdeh, Composites with functionally graded interphases: Mesocontinuum concept and effective transverse conductivity, Acta Materialia 44 (5) (1996) 2057 – 2066. doi:https://doi.org/10.1016/1359-6454(95)00269-3.

[50] M. Ostoja-Starzewski, Microstructural disorder, mesoscale finite elements and macroscopic response, Proceedings of the Royal Society of London. Series A: Mathematical, Physical and Engineering Sciences 455 (1989) (1999) 3189–3199. doi:10.1098/rspa.1999.0446.

[51] M. Ostoja-Starzewski, Microstructural Randomness and Scaling in Mechanics of Materials, Taylor and Francis, Abingdon, 2007.
URL https://cds.cern.ch/record/1086189

[52] M. Ostoja-Starzewski, J. Schulte, Bounding of effective thermal conductivities of multiscale materials by essential and natural boundary conditions, Phys. Rev. B 54 (1996) 278–285. doi:10.1103/PhysRevB.54.278.

[53] A. Saharan, M. Ostoja-Starzewski, S. Koric, Fractal Geometric Characterization of Functionally Graded Materials, Journal of Nanomechanics and Micromechanics 3 (4) (2013) 04013001. doi:10.1061/(ASCE)NM.2153-5477.0000058.

[54] B. Uymaz, M. Aydogdu, Three-dimensional vibration analyses of functionally graded plates under various boundary conditions, Journal of Reinforced Plastics and Composites 26 (18) (2007) 1847–1863.

CAPTIONS OF TABLES

Table 1: Shape functions with different BCs.

Table 2: Material properties of the FG plates

Table 3: Convergence study of Al/ZrO_2-2 square plates subjected to a uniformly distributed load ($a/h = 5$, $p = 2$).

Table 4: Nondimensional stresses and displacements of simply-supported Al/Al_2O_3 square plates under a sinusoidal load with $a/h = 10$.

Table 5: Nondimensional deflections ($\hat{w}$) of Al/ZrO_2-1 square plates under a uniformly distributed load with different BCs.

Table 6: Nondimensional fundamental frequency ($\bar{\omega}$) of Al/ZrO_2-2 square plates with different BCs.

Table 7: Critical buckling temperatures ($\bar{T}_{cr}$) of simply-supported Al/Al_2O_3 square plates.

CAPTIONS OF FIGURES

Figure 1: Geometry of a FG plate.

Figure 2: Variation of transverse shear stress $\bar{\sigma}_{xz}$ in the thickness direction with respect to p of simply-supported Al/ZrO_2-1 plate under a uniformly distributed load ($a/h = 10$).

Figure 3: Variation of membrane stress $\bar{\sigma}_x$ in the thickness direction with respect to p of simply-supported Al/ZrO_2-1 plate under a uniformly distributed load ($a/h = 10$).

Figure 4: Variation of nondimensional center deflection $\hat{w}$ of Al/ZrO_2-1 plate under uniformly distributed load with respect to a/h and p.

Figure 5: Variation of the critical buckling temperatures of Al/Al_2O_3 plate with respect to p for the UTR and different BCs ($a/h = 10$).

Figure 6: Variation of the critical buckling temperatures of simply-supported Al/Al_2O_3 plate with respect to p and different temperature rises ($a/h = 10$, SSSS).

Figure 7: Variation of nondimensional fundamental frequency of simply-supported Al/Al_2O_3 plate with respect to the different temperature rises ($a/h = 5$, $p = 5$).

Table 1: Shape functions with different BCs.

Boundary conditions	Shape functions	
	$R_j(x)$	$P_j(y)$
SSSS	$x(a-x)e^{-\frac{jx}{a}}$	$y(b-y)e^{-\frac{jy}{b}}$
CCCC	$x^2(a-x)^2e^{-\frac{jx}{a}}$	$y^2(y-b)^2e^{-\frac{jy}{b}}$
CCSS	$x^2(a-x)^2e^{-\frac{jx}{a}}$	$y(b-y)e^{-\frac{jy}{b}}$
CSCS	$x^2(a-x)e^{-\frac{jx}{a}}$	$y^2(b-y)e^{-\frac{jy}{b}}$
CCSF	$x^2(a-x)^2e^{-\frac{jx}{a}}$	$ye^{-\frac{jy}{b}}$
CCFF	$x^2(a-x)^2e^{-\frac{jx}{a}}$	$e^{-\frac{jy}{b}}$

Table 2: Material properties of the FG plates

Material	E (GPa)	ρ (kg/m^3)	ν	α (1/C)	k (W/mK)
Aluminum (Al)	70	2702	0.3	23×10^{-6}	204
Zirconia (ZrO_2-1)	200	5700	0.3	-	-
Zirconia (ZrO_2-2)	151	3000	0.3	-	-
Alumina (Al_2O_3)	380	3800	0.3	7.4×10^{-6}	10.4

Table 3: Convergence study of Al/ZrO_2-2 square plates subjected to a uniformly distributed load with different BCs. ($a/h = 5$, $p = 2$).

BCs	Number of series							
	1	2	4	6	8	10	12	14
Center transverse displacement ($\hat{w}$)								
SSSS	0.3429	0.6411	0.6379	0.6383	0.6376	0.6375	0.6372	0.6373
CCCC	0.2331	0.2654	0.2563	0.2650	0.2629	0.2693	0.2685	0.2683
CCSS	0.2733	0.3690	0.3664	0.3740	0.3724	0.3763	0.3753	0.3743
CSCS	0.3483	0.3856	0.3813	0.3849	0.3837	0.3843	0.3864	0.3865
CCFF	0.3694	0.4898	0.4846	0.4942	0.4942	0.4957	0.4984	0.4977
CCSF	0.3700	0.4216	0.4230	0.4373	0.4357	0.4406	0.4402	0.4409
Fundamental frequency ($\bar{\omega}$)								
SSSS	1.9077	1.4789	1.4691	1.4666	1.4669	1.4666	1.4666	1.4666
CCCC	2.4714	2.3717	2.2964	2.2729	2.2742	2.2681	2.2697	2.2687
CCSS	2.2057	1.9746	1.9230	1.9066	1.9075	1.9039	1.9050	1.9048
CSCS	1.9486	1.9087	1.8688	1.8636	1.8622	1.8615	1.8609	1.8606
CCFF	1.6430	1.5500	1.5061	1.4934	1.4938	1.4920	1.4929	1.4921
CCSF	1.7340	1.6256	1.5758	1.5577	1.5583	1.5549	1.5553	1.5557

Table 4: Nondimensional stresses and displacements of simply-supported Al/Al_2O_3 square plates under a sinusoidal load ($a/h = 10$).

p	Theory	$\bar{u}(-h/4)$	$\bar{w}$	$\bar{\sigma}_x(h/3)$	$\bar{\sigma}_{xy}(-h/3)$	$\bar{\sigma}_{xz}(h/6)$
1	Present	0.6416	0.5890	1.4888	0.6140	0.2551
	HSDT [6]	0.6414	0.5890	1.4898	0.6111	0.2608
	SSDT [5]	0.6626	0.5889	1.4894	0.6110	0.2622
	Quasi-3D [11]	0.6436	0.5875	1.5062	0.6081	0.2510
2	Present	0.8986	0.7573	1.3950	0.5469	0.2704
	HSDT [6]	0.8984	0.7573	1.3960	0.5442	0.2737
	SSDT [5]	0.9281	0.7573	1.3954	0.5441	0.2763
	Quasi-3D [11]	0.9012	0.7570	1.4147	0.5421	0.2496
4	Present	1.0497	0.8815	1.1783	0.5719	0.2528
	HSDT [6]	1.0502	0.8815	1.1794	0.5669	0.2537
	SSDT [5]	1.0941	0.8819	1.1783	0.5667	0.2580
	Quasi-3D [11]	1.0541	0.8823	1.1985	0.5666	0.2362
8	Present	1.0764	0.9746	0.9467	0.5926	0.2084
	HSDT [6]	1.0763	0.9746	0.9477	0.5858	0.2088
	SSDT [5]	1.1340	0.9750	0.9466	0.5856	0.2121
	Quasi-3D [11]	1.0830	0.9738	0.9687	0.5879	0.2262

Table 5: Nondimensional deflections ($\hat{w}$) of Al/ZrO_2-1 square plates under a uniformly distributed load with different BCs.

a/h	BCs	Theory	p					
			0	0.5	1	2	5	10
5	SSSS	Present	0.1716	0.2324	0.2719	0.3135	0.3568	0.3871
		FSDT [3]	0.1722	0.2403	0.2811	0.3221	-	-
		FSDT [2]	0.1701	0.2232	0.2521	0.2825	-	-
		Quasi-3D [8]	0.1671	0.2505	0.2905	0.3280	-	-
	CCCC	Present	0.0741	0.0985	0.1153	0.1354	0.1600	0.1743
		FSDT [3]	0.0774	0.1073	0.1207	0.1404	-	-
		FSDT [2]	0.0750	0.0975	0.1109	0.1264	-	-
		Quasi-3D [8]	0.0731	0.1034	0.1253	0.1444	-	-
	CCSS	Present	0.1029	0.1376	0.1610	0.1881	0.2201	0.2395
	CSCS	Present	0.1046	0.1402	0.1643	0.1910	0.2219	0.2413
		FSDT [3]	0.1073	0.1447	0.1701	0.1953	-	-
		Quasi-3D [8]	0.1017	0.1501	0.1751	0.2008	-	-
	CCFF	Present	0.1357	0.1811	0.2121	0.2480	0.2906	0.3164
	CCSF	Present	0.1206	0.1612	0.1885	0.2205	0.2583	0.2812
10	SSSS	Present	0.1495	0.2045	0.2391	0.2730	0.3039	0.3288
	CCCC	Present	0.0521	0.0707	0.0827	0.0952	0.1079	0.1170
	CCSS	Present	0.0765	0.1041	0.1218	0.1398	0.1577	0.1709
	CSCS	Present	0.0817	0.1113	0.1302	0.1492	0.1675	0.1814
	CCFF	Present	0.1017	0.1382	0.1618	0.1858	0.2094	0.2269
	CCSF	Present	0.0896	0.1218	0.1424	0.1636	0.1845	0.1999

Table 6: Nondimensional fundamental frequency ($\bar{\omega}$) of Al/ZrO_2-2 square plates with different BCs..

BCs	a/h	Theory	p					
			0	0.5	1	2	5	10
SSSS	5	Present	1.7761	1.6026	1.5277	1.4666	1.4127	1.3757
		HSDT [7]	1.7723	1.6003	1.5245	1.4629	1.4084	1.3726
		3D [54]	1.7748	1.6031	1.4764	1.4628	1.4106	1.3711
	10	Present	1.9325	1.7385	1.6589	1.5993	1.5501	1.5091
		HSDT [7]	1.9330	1.7402	1.6593	1.5994	1.5500	1.5095
		3D [54]	1.9339	1.7406	1.6583	1.5968	1.5491	1.5066
CCCC	5	Present	2.7535	2.5006	2.3810	2.2683	2.1580	2.1011
		3D [54]	2.7404	2.4919	2.3706	2.2561	2.1447	2.0832
	10	Present	3.3219	2.9974	2.8582	2.7460	2.6463	2.5760
		3D [54]	3.3496	3.0249	2.8809	2.7658	2.6645	2.5923
CCSS	5	Present	2.3102	2.0945	1.9946	1.9041	1.8174	1.7698
		3D [54]	2.3000	2.0880	1.9849	1.8947	1.8055	1.7549
	10	Present	2.7177	2.4502	2.3366	2.2467	2.1686	2.1111
		3D [54]	2.7349	2.4678	2.3516	2.2605	2.1794	2.1213
CCFF	5	Present	1.8094	1.6411	1.5630	1.4920	1.4236	1.3859
		3D [54]	1.8110	1.6431	1.5620	1.4899	1.4212	1.3820
	10	Present	2.1049	1.8973	1.8095	1.7406	1.6812	1.6355
		3D [54]	2.1260	1.9183	1.8275	1.7549	1.6941	1.6492
CCSF	5	Present	1.8861	1.7106	1.6292	1.5549	1.4832	1.4441
		3D [54]	1.8841	1.7088	1.6248	1.5491	1.4798	1.4352
	10	Present	2.2102	1.9923	1.9002	1.8276	1.7642	1.7173
		3D [54]	2.2271	2.0099	1.9131	1.8411	1.7748	1.7291

Table 7: Critical buckling temperatures ($\bar{T}_{cr}$) of simply-supported Al/Al_2O_3 square plates.

Temperature rise	a/h	Theory	p					
			0	0.5	1	2	5	10
UTR	5	Present	5.5839	3.2409	2.6717	2.3410	2.2745	2.2780
		FSDT [4]	5.5806	-	-	-	2.3594	2.3682
		HSDT [9]	5.5834	-	2.6715	-	2.2750	2.2767
		Quasi-3D [9]	5.8781	-	2.8661	-	2.4396	2.4162
	10	Present	1.6188	0.9243	0.7584	0.6701	0.6793	0.6932
		FSDT [4]	1.6186	-	-	-	0.6867	0.7010
		HSDT [9]	1.6186	-	0.7583	-	0.6793	0.6926
		Quasi-3D [9]	1.6444	-	0.7908	-	0.7137	0.7177
LTR	5	Present	11.1678	6.4681	5.0107	4.1209	3.9154	4.0393
		FSDT [4]	11.1513	-	-	-	4.0527	4.1877
		HSDT [9]	11.1568	-	5.0009	-	3.9073	4.0257
		Quasi-3D [9]	11.7462	-	5.3659	-	4.1907	4.2728
	10	Present	3.2376	1.8447	1.4224	1.1797	1.1694	1.2291
		FSDT [4]	3.2272	-	-	-	1.1735	1.2335
		HSDT [9]	3.2273	-	1.4129	-	1.1606	1.2186
		Quasi-3D [9]	3.2788	-	1.4738	-	1.2199	1.2630
NLTR	5	Present	11.1678	11.2724	8.9162	6.8685	5.5074	5.0212
		FSDT [4]	11.1513	-	-	-	5.0685	4.8402
	10	Present	3.2376	3.2149	2.5311	1.9662	1.6449	1.5279
		FSDT [4]	3.2272	-	-	-	1.4676	1.4256

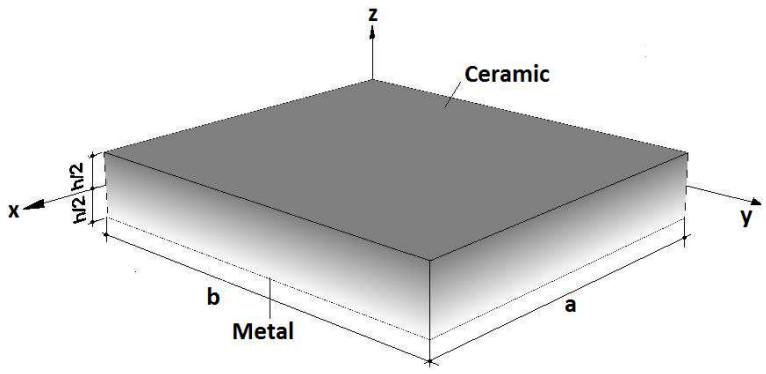

Figure 1: Geometry of a FG plate.

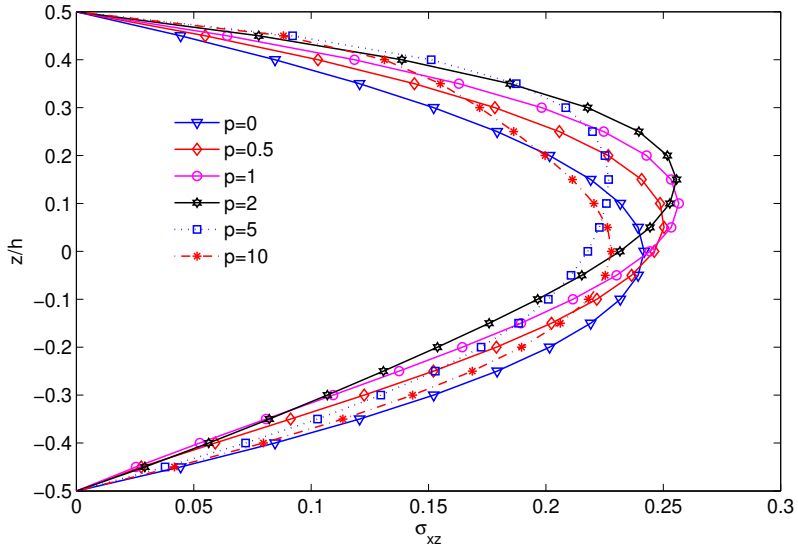

Figure 2: Variation of transverse shear stress $\bar{\sigma}_{xz}$ in the thickness direction with respect to p of simply-supported Al/ZrO_2-1 plate under a uniformly distributed load ($a/h = 10$).

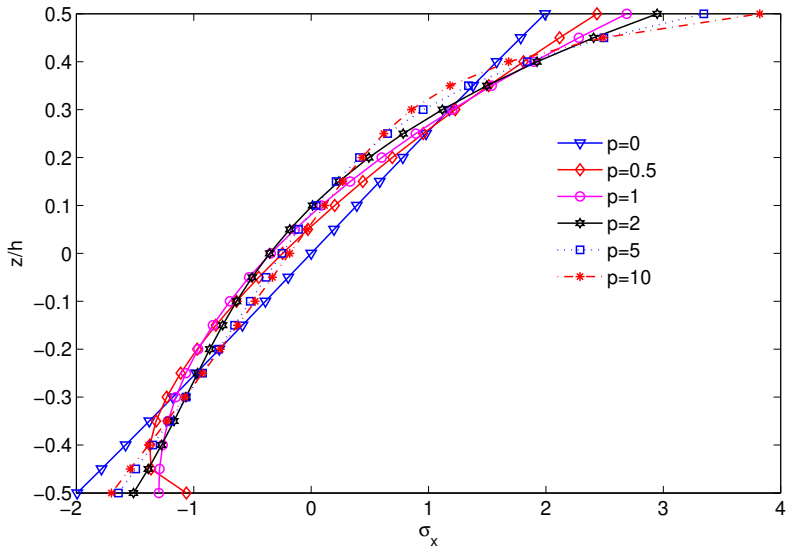

Figure 3: Variation of membrane stress $\bar{\sigma}_x$ in the thickness direction with respect to p of simply-supported Al/ZrO_2-1 plate under a uniformly distributed load ($a/h = 10$).

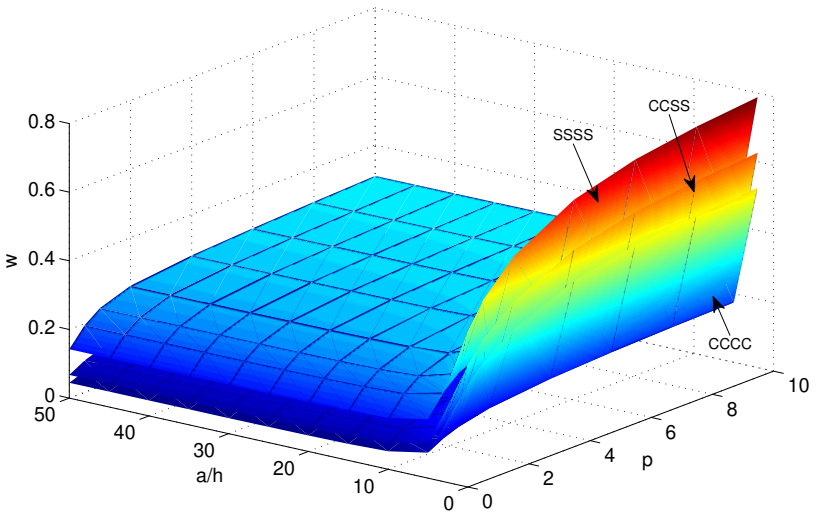

Figure 4: Variation of nondimensional center deflection $\hat{w}$ of Al/ZrO_2-1 plate under uniformly distributed load with respect to a/h and p.

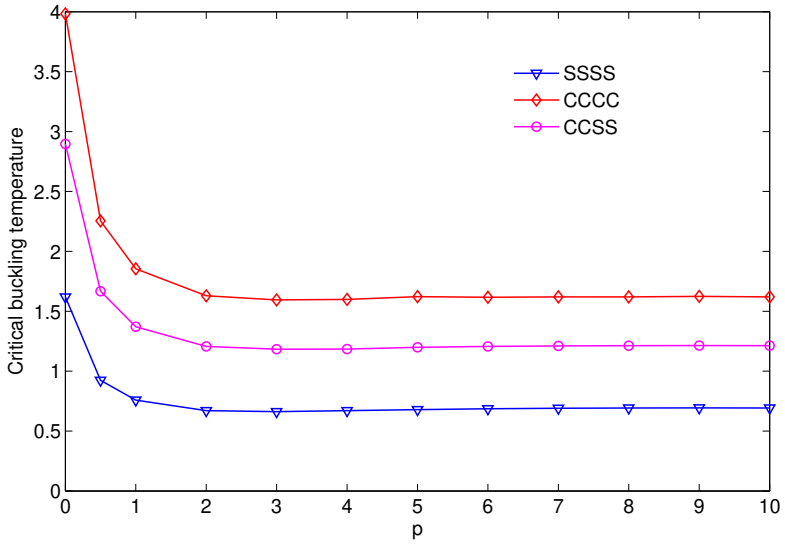

Figure 5: Variation of the critical buckling temperatures of Al/Al_2O_3 plate with respect to p for the UTR and different BCs ($a/h = 10$).

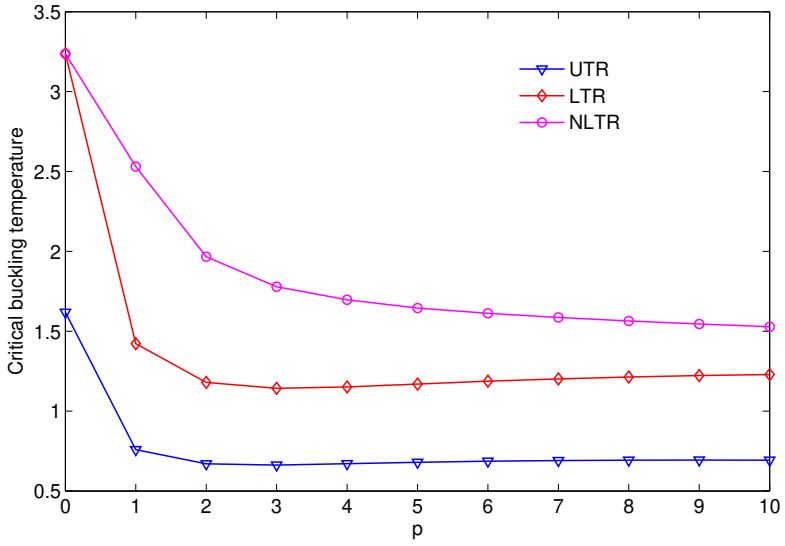

Figure 6: Variation of the critical buckling temperatures of simply-supported Al/Al_2O_3 plate with respect to p and different temperature rises ($a/h = 10$).)

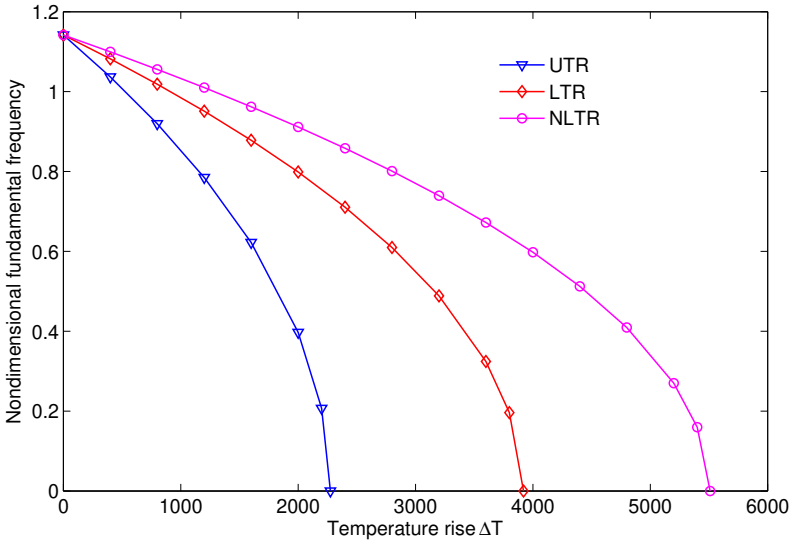

Figure 7: Variation of nondimensional fundamental frequency of simply-supported Al/Al_2O_3 plate with respect to the different temperature rises ($a/h = 5$, $p = 5$).